

Interpreting LHC Higgs Results from Natural New Physics Perspective

Dean Carmi^a, Adam Falkowski^b, Eric Kuflik^a, and Tomer Volansky^a

^a *Raymond and Beverly Sackler School of Physics and Astronomy, Tel-Aviv University,
Tel-Aviv 69978, Israel*

^b *Laboratoire de Physique Théorique d'Orsay, UMR8627-CNRS,
Université Paris-Sud, Orsay, France*

Abstract

We analyze the 2011 LHC Higgs data in the context of simplified new physics models addressing the naturalness problem. These models are expected to contain new particles with sizable couplings to the Higgs boson, which can easily modify the Higgs production cross sections and branching fractions. We focus on searches in the $h \rightarrow ZZ^* \rightarrow 4l$ and $h \rightarrow \gamma\gamma$ channels, in the latter case including the vector boson fusion production mode. Combining the available ATLAS and CMS data in these channels, we derive constraints on an effective low-energy theory of the Higgs boson. We then map several simplified scenarios to the effective theory, capturing numerous natural new physics models such as supersymmetry and Little Higgs, and extract the constraints on the corresponding parameter space. We show that simple models where one fermionic or one scalar partner is responsible for stabilizing the Higgs potential are already constrained in a non-trivial way by LHC Higgs data.

1 Introduction

Discovering the Higgs boson and measuring its mass and branching ratios is one of the key objectives of the LHC. Within the Standard Model (SM), the coupling to the Higgs boson is completely fixed by the particle mass. This is no longer the case in many scenarios beyond the SM, where the Higgs couplings to the SM gauge bosons and fermions may display sizable departures from the SM predictions. Indeed, precision studies of the Higgs couplings may be the shortest route to new physics.

Interestingly, from this point of view, a Higgs boson in the range $115 - 130$ GeV is particularly well suited as a new physics probe. One reason is that several different Higgs decay channels, in particular the $\gamma\gamma$, ZZ^* and WW^* channels, can be realistically accessed by experiment. The first of these arises in the SM at one loop and, consequently, physics beyond the SM may easily modify its rate. This is especially true in models addressing the naturalness problem of electroweak symmetry breaking, which necessarily contain new charged particles with significant couplings to the Higgs boson. Well-known examples where this is the case include supersymmetric or composite Higgs models. Furthermore, the tree-level Higgs coupling to WW and ZZ is often modified as well, as is the case in composite or multi-Higgs models. Similar comments apply to the Higgs production rate: the dominant production mode via gluon fusion is a one loop process in the SM and is therefore particularly sensitive to new physics containing, as in typical natural models, light new colored states coupled to the Higgs. Subleading production modes, such as vector boson fusion (VBF), may also be affected.

While several Higgs production and decay modes may change in the presence of new particles, the correlated change in different channel may crucially depend on the new physics scenario. Consequently, a joint analysis of distinct independent channels may either allow to place interesting bounds on new physics scenarios or otherwise provide a way to discover new physics and pinpoint its identity. The goal of this paper is to demonstrate the above understanding in light of the new Higgs measurements at ATLAS and CMS, and place constraints on new physics models which solve the fine-tuning problem.

Recently, ATLAS and CMS have reported the results of Higgs searches based on 5 fb^{-1} of data in several channels [1, 2, 3, 4, 5, 6]. The results, albeit inconclusive, suggest the

existence of a Higgs boson with mass near 125 GeV manifesting itself in the diphoton and 4-lepton final states. It is therefore natural to try and answer the following question: *Assuming a Higgs boson with the mass $120 \text{ GeV} \leq m_h \leq 130 \text{ GeV}$, what are the implications of these results for natural models beyond the SM?* Below we pursue this question.

We combine the latest ATLAS and CMS Higgs results in three channels: diphoton and 4-leptons through gluon fusion, and diphoton through VBF. Our focus is to interpret the LHC results in terms of simple (sometimes simplified) models that address the fine-tuning problem in the sense of providing a new contribution to the Higgs mass that cancels the quadratically divergent contribution of the SM top quark. To do so, we first consider the Higgs effective action at low energy and derive the constraints on its couplings. We then map various theories onto the effective action to extract their bounds. A number of partly overlapping papers have recently investigated the 125 GeV Higgs-like excess in the context of composite Higgs [7], supersymmetric Higgs [8], and multi-Higgs models [9]; see also [10]. For earlier related work, see [11].

Of course, at this stage the limited statistical power of the current Higgs data does not allow us to make a strong statement about any new physics scenario. Nevertheless, in several cases we are able to identify non-trivial regions of the parameter space that are disfavored at 90% CL. Repeating this analysis with future data may allow us, in the best case scenario, to pinpoint departures of the Higgs couplings from the SM predictions. That would not only provide evidence of new physics, but also some information about its scale, thereby supplying important hints about the nature of the fundamental theory at the electroweak scale.

The paper is organized as follows. In the next section we define the effective action for a Higgs boson interacting with the SM fields and identify the relevant parameters that are being constrained by the present data. In Section 3 we discuss the LHC data and provide the combined best-fit of the ATLAS and CMS Higgs results for the three channels discussed above. We then show the resulting constraints on the parameters of the Higgs effective action. In Section 4 we then study simplified models with scalar top partners, relevant for the MSSM as well. Section 5 focuses on fermionic top partners which show up in many composite Higgs and Little Higgs models. Several representative examples are discussed. Section 6 discusses some implications of theories with 2 Higgs particles. We conclude in

Section 7.

2 Formalism

We begin by defining a convenient framework to describe LHC Higgs phenomenology. We define an effective theory at the scale $\mu \sim m_h$, which describes the couplings of a single Higgs boson, h , to the SM gauge bosons and fermions. Keeping dimension 5 operators and writing only couplings to the heaviest fermions we have,

$$\begin{aligned} \mathcal{L}_{eff} = & c_V \frac{2m_W^2}{v} h W_\mu^+ W_\mu^- + c_V \frac{m_Z^2}{v} h Z_\mu Z_\mu - c_b \frac{m_b}{v} h \bar{b}b - c_\tau \frac{m_\tau}{v} h \bar{\tau}\tau \\ & + c_g \frac{\alpha_s}{12\pi v} h G_{\mu\nu}^a G_{\mu\nu}^a + c_\gamma \frac{\alpha}{\pi v} h A_{\mu\nu} A_{\mu\nu}. \end{aligned} \quad (2.1)$$

Here $v = 246$ GeV, and $G_{\mu\nu}^a$ and $A_{\mu\nu}$ are the field strengths of the gluon and photon, respectively. The fact that the same parameter c_V controls the coupling to W and Z boson follows from the assumption that these couplings respect, to a good approximation, custodial symmetry, as strongly suggested by electroweak precision observables. We note that the Higgs could decay to particles from beyond the SM, e.g. to invisible collider-stable particles, but we will not discuss this possibility here. We further note that while a single Higgs is kept at low energy, the above may describe multi-Higgs models, as long as there is a sizable splitting between the lightest and the remaining Higgs fields. We study such a possibility in more detail in Section 6.

In (2.1), the top quark has been integrated out, contributing at 1-loop to c_g and c_γ as

$$c_g(\tau_t) = c_t A_f(\tau_t), \quad c_\gamma(\tau_t) = \frac{2c_t}{9} A_f(\tau_t), \quad A_f(\tau) = \frac{3}{2\tau^2} [(\tau - 1)f(\tau) + \tau], \quad (2.2)$$

where $\tau_t = m_h^2/4m_t^2$, c_t is the ratio of the top-Higgs Yukawa coupling to the SM one, and

$$f(\tau) = \begin{cases} \arcsin^2 \sqrt{\tau} & \tau \leq 1 \\ -\frac{1}{4} \left[\log \frac{1+\sqrt{1-\tau^{-1}}}{1-\sqrt{1-\tau^{-1}}} - i\pi \right]^2 & \tau > 1 \end{cases}. \quad (2.3)$$

For $m_h^2 \ll 4m_t^2$ one finds, $f(\tau) \simeq \tau(1 + \tau/3)$, which is a very good approximation for $m_h \lesssim 130$ GeV. Consequently, for the SM with a light Higgs boson matched to our effective theory at 1-loop we have

$$c_{V,\text{SM}} = c_{b,\text{SM}} = 1, \quad c_{g,\text{SM}} \simeq 1, \quad c_{\gamma,\text{SM}} \simeq 2/9. \quad (2.4)$$

The decay widths of the Higgs relative to the SM predictions are modified approximately as,

$$\begin{aligned} \frac{\Gamma(h \rightarrow b\bar{b})}{\Gamma_{SM}(h \rightarrow b\bar{b})} &= |c_b|^2, & \frac{\Gamma(h \rightarrow WW^*)}{\Gamma_{SM}(h \rightarrow WW^*)} &= \frac{\Gamma(h \rightarrow ZZ^*)}{\Gamma_{SM}(h \rightarrow ZZ^*)} = |c_V|^2, \\ \frac{\Gamma(h \rightarrow gg)}{\Gamma_{SM}(h \rightarrow gg)} &\simeq |c_g|^2, & \frac{\Gamma(h \rightarrow \gamma\gamma)}{\Gamma_{SM}(h \rightarrow \gamma\gamma)} &= \left| \frac{\hat{c}_\gamma}{\hat{c}_{\gamma,SM}} \right|^2, \end{aligned} \quad (2.5)$$

where \hat{c}_γ includes also the one-loop contribution due to the triangle diagram with the W boson¹,

$$\hat{c}_\gamma(\tau_t, \tau_W) = c_\gamma(\tau_t) - \frac{c_V}{8\tau_W^2} [3(2\tau_W - 1)f(\tau_W) + 3\tau_W + 2\tau_W^2], \quad (2.6)$$

where $\tau_W = m_h^2/4m_W^2$. For $m_h = 125$ GeV one finds $\hat{c}_\gamma \simeq c_\gamma - 1.04c_V$, and thus $\hat{c}_{\gamma,SM} \simeq -0.81$.

More generally, the 1-loop contribution to c_g from an additional fermion in the fundamental representation of color $SU(3)$ and coupled to the Higgs via the Yukawa coupling $y_f h \bar{f}/\sqrt{2}$ is simply given by Eq. (2.2) with $c_t \rightarrow (vy_f/\sqrt{2}m_f)$ and $\tau_t \rightarrow \tau_f$, while for an $SU(3)_C$ fundamental scalar,

$$\delta c_g(\tau_s) = \frac{1}{4} \sum_s g_{hss} A_s(\tau_s), \quad g_{hss} = \frac{1}{2} \frac{v}{m_s^2} \frac{\partial m_s^2}{\partial v}, \quad A_s(\tau) = \frac{3}{\tau^2} [f(\tau) - \tau]. \quad (2.7)$$

For the photon coupling we have

$$\delta c_\gamma(\tau_{f,s}) = \frac{Q_{f,s}^2}{2} \delta c_g(\tau_{f,s}), \quad (2.8)$$

where $Q_{f,s}$ is the electric charge of the scalar or fermion. More general expressions can be found e.g in [12]. Note that in the limit $\tau \rightarrow 0$, $A_{f,s}(\tau) \rightarrow 1$, and the scalar contribution becomes 1/4 that of the fermion. In fact, the $\tau \rightarrow 0$ limit is equivalent to approximating c_g and c_γ using the 1-loop beta function [13], which explains the relative factor 1/4.

As discussed in the introduction, the most significant constraints on the effective theory are obtained by studying several independent Higgs decay channels. The three most constraining channels studied by ATLAS and CMS to date are $h \rightarrow ZZ^*$, $h \rightarrow \gamma\gamma$ and $pp \rightarrow hjj \rightarrow \gamma\gamma jj$. The Higgs production mechanism in the first two channels is dominated

¹There are additional one-loop contributions to c_γ and c_g from light quarks that are left out in this discussion, but are included in the analyses below.

by the gluon fusion process which scales as c_g^2 , while the last process, which is dominated by VBF², scales as c_V^2 . On the other hand, the decays of a light Higgs are dominated by decays to b-quarks, scaling roughly as c_b^2 . With these approximations, the relevant Higgs event rates scale as,

$$R_V \equiv \frac{\sigma(pp \rightarrow h)\text{Br}(h \rightarrow ZZ^*)}{\sigma_{SM}(pp \rightarrow h)\text{Br}_{SM}(h \rightarrow ZZ^*)} \simeq \left| \frac{c_g c_V}{c_b} \right|^2, \quad (2.9)$$

$$R_\gamma \equiv \frac{\sigma(pp \rightarrow h)\text{Br}(h \rightarrow \gamma\gamma)}{\sigma_{SM}(pp \rightarrow h)\text{Br}_{SM}(h \rightarrow \gamma\gamma)} \simeq \left| \frac{c_g \hat{c}_\gamma}{\hat{c}_{\gamma,SM} c_b} \right|^2, \quad (2.10)$$

$$R_{\gamma,VBF} \equiv \frac{\sigma(pp \rightarrow h jj)\text{Br}(h \rightarrow \gamma\gamma)}{\sigma_{SM}(pp \rightarrow h jj)\text{Br}_{SM}(h \rightarrow \gamma\gamma)} \simeq \left| \frac{c_V \hat{c}_\gamma}{\hat{c}_{\gamma,SM} c_b} \right|^2. \quad (2.11)$$

The Higgs rate is the same in the WW and ZZ channels as a consequence of custodial symmetry. Because the former channel was not updated by ATLAS to the full 5 fb⁻¹ dataset, below we restrict our analysis to the $h \rightarrow ZZ^* \rightarrow 4l$ channel which is currently more sensitive. Note that if the $h \rightarrow \gamma\gamma$ decay width is dominated by the W boson loop contribution, as in the SM, then $\hat{c}_\gamma \sim c_V$ and the Higgs event rates in the first two channels are modified by approximately the same factor. In this case, the 2011 Higgs data can be described by only two parameters: the overall rescaling of the production rate in the first two channels, $\hat{\mu}_g = |c_g c_V / c_b|^2$, and the rescaling of the VBF channel, $\hat{\mu}_{VBF} = |c_V^2 / c_b|^2$. On the other hand, if there are new important contributions to c_γ , for example from new light charged particles, or due to a reduction of the Higgs coupling to WW and ZZ , then the Higgs data depend on the three combinations of parameters in (2.9)-(2.11). In the next sections, we construct the bounds on these rates.

3 Constraints from the LHC

Recently, ATLAS and CMS have reported the results of Higgs searches in several channels. Here we focus on the $h \rightarrow \gamma\gamma$ [2, 4] and $h \rightarrow ZZ^* \rightarrow 4l$ [3, 5] channels, which are currently the most sensitive ones for $115 < m_h < 130$ GeV. Notably, both experiments observe an

²The Higgs production via gluon fusion also contributes to the $2\gamma 2j$ final state studied by CMS. In the SM, its contribution is about 1/3 that of the VBF production mode [4], but it may become more important in models where the gluon fusion cross section is enhanced relative to the VBF one. In the following we take this into account in our fits. We thank Yevgeny Kats for pointing this out to us.

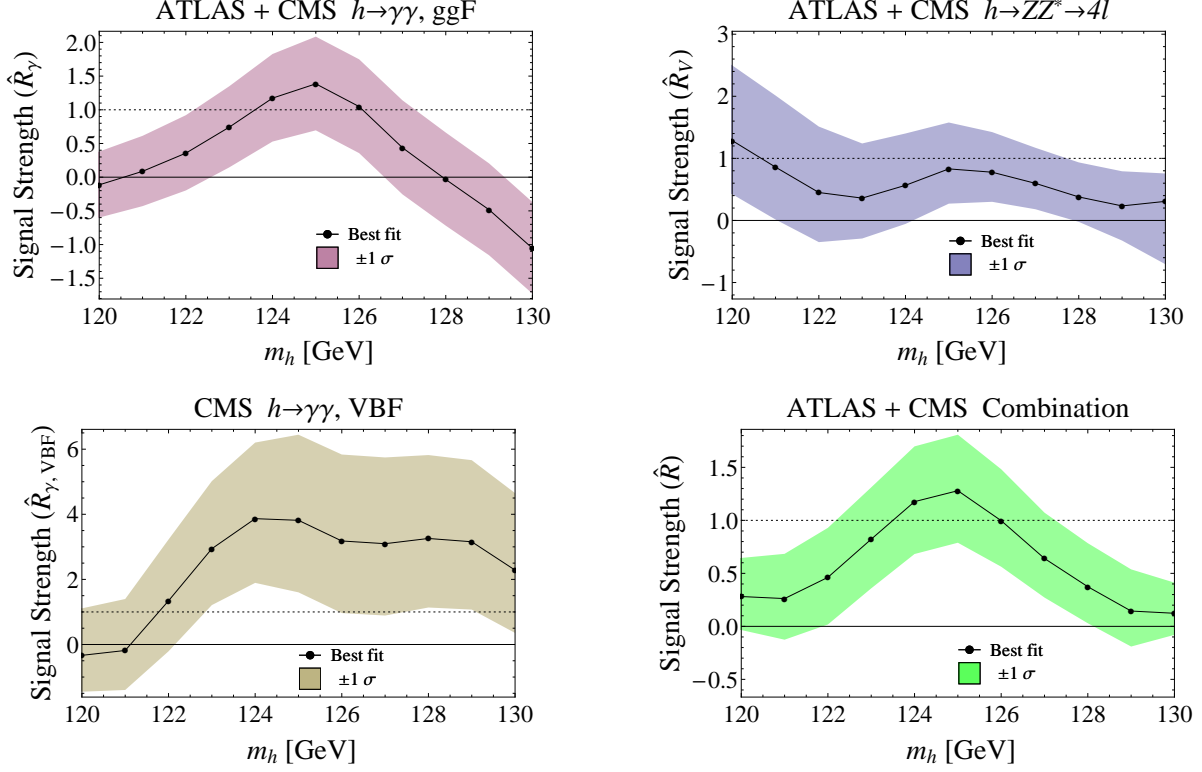


Figure 1: Combined best-fit values and 1σ bands, obtained for each of the gluon fusion (ggF) channels (**top-left:** diphoton, **top-right:** 4-lepton), and the CMS fit for VBF diphoton channel (**bottom-left**), for a Higgs mass between 120 GeV and 130 GeV. We also show the combination of all three channels (**bottom-right**). In all fits the likelihood was computed without taking into account systematic uncertainties which are not expected to alter the results significantly. Nonetheless, comparing our 1σ bands to published ATLAS or CMS results before combination our results can be shown to be quite conservative. See text for more details.

excess of events in these channels that (inconclusively) indicate the existence of a Higgs boson with mass in the 124 – 126 GeV range. In fact, the $h \rightarrow ZZ^*$ channel at ATLAS and $h \rightarrow \gamma\gamma$ channel in both experiments hint towards a somewhat large production rate, a factor of two to four larger than that expected in the SM. In particular, CMS reports an excess of events in the VBF production mode in the diphoton channel near $m_h \sim 124$ GeV which is larger than expected from the SM. However, the best fit value for the Higgs mass differs between the two experiments by roughly 2 GeV. Consequently, as will be shown below, combining the results together points to a production cross-section and branching fractions similar to that predicted by the SM. It remains to be seen whether with better statistics and improved understanding of the systematics, the results will remain consistent with the SM prediction, or otherwise converge on a rate deviating from that predicted by the SM.

In order to constrain the couplings of the effective theory – c_g, c_γ, c_V, c_b and c_τ in Eq. (2.1) – it is crucial to analyze several Higgs production and decay modes. Following the discussion above, we focus on the channels which observe a clear excess of Higgs-like events: the gluon fusion initiated $pp \rightarrow h \rightarrow ZZ^* \rightarrow 4l$, $pp \rightarrow h \rightarrow \gamma\gamma$, and the vector-boson-fusion initiated $pp \rightarrow hjj \rightarrow \gamma\gamma jj$. Since one of the production modes (gluon fusion) and one of the decay modes ($\gamma\gamma$) are loop-induced, these constraints are very sensitive to heavy particles beyond the SM that may play a role in solving the fine tuning problem, leading to interesting conclusions on new physics and naturalness.

For each channel, it is ideal to combine the constraints from ATLAS and CMS. Unfortunately, the two experiments do not provide sufficient information that allow for a shared analysis. Therefore, we repeat the analyses, computing, and then combining, the likelihood functions in each search. Where possible, we use background and signal modeling given by the experiments, normalizing the signal to the reported values. In the remaining cases we simulate the signal using Madgraph [14] and Delphes [15], and implement the reported cuts. For the results shown here, we do not take into account the systematic effects which are expected to be small³. In Fig. 1 we show the results of the combined best fit value of $\hat{R} \equiv \sigma/\sigma_{\text{SM}}$, for each of the three analyzed channels separately and for the combination of

³We have checked in some cases that the effect of taking into account the systematics is negligible, at the percent level.

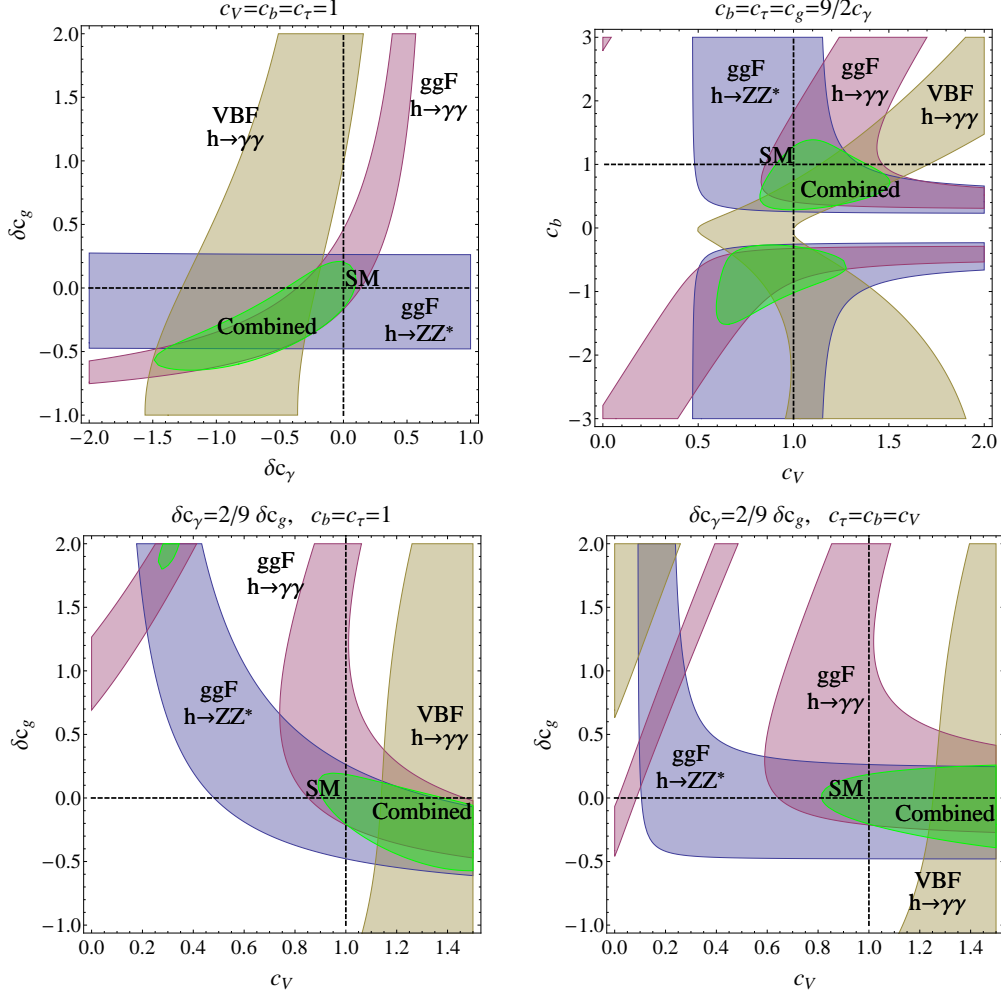


Figure 2: The allowed parameter space of the effective theory given in Eq. (2.1), derived from the combined ATLAS and CMS constraints for $m_h = 125$ GeV. We display the 1σ allowed regions generated from Higgs produced via gluon fusion (ggF) decaying to $\gamma\gamma$ (pink), or to $ZZ^* \rightarrow 4l$ (blue), and Higgs produced via vector boson fusion (VBF) decaying to $\gamma\gamma$ (beige). The “Combined” region (green) shows the 90% CL allowed region arising from all channels. The dashed lines show the SM values. The top left plot characterizes models in which loops containing beyond the SM fields contribute to the effective 5-dimensional $h G_{\mu\nu}^a G_{\mu\nu}^a$ and $h A_{\mu\nu} A_{\mu\nu}$ operators, while leaving the lower-dimension Higgs couplings in Eq. (2.1) unchanged relative to the SM prediction. The remaining plots characterize *top partner* models where only scalars and fermions with the same charge and color as the top quark contribute to the effective 5-dimensional operators, which implies the relation $\delta c_\gamma = (2/9)\delta c_g$. The results are shown for 3 different sets of assumptions about the lower-dimension Higgs couplings that can be realized in concrete models addressing the Higgs naturalness problem. The top right plot was added in v2 to allow a direct comparison with the results of Refs. [27] and [28].

all three channels. We vary the Higgs mass between 120 GeV and 130 GeV. The bands indicate the 1σ uncertainty. For $m_h \approx 125$ GeV, which we find best explains the combined measurements, the best fit cross-section is consistent with the SM cross-section.

In all of our results, our estimation of the 1-sigma band for $\hat{\mu}$ is larger than that reported by the individual experiments. From this point of view, our results are expected to be conservative and the constraints based on the prospective official ATLAS/CMS combination may be stronger than those reported here. Our procedure does not (and cannot) take into account some important information and should therefore be taken with a grain of salt.

We use our results of Fig. 1, and place constraints on the effective theory. In Fig. 2 we show two dimensional constraints on $\delta c_g = c_g - c_{g,\text{SM}}$, $\delta c_\gamma = c_\gamma - c_{\gamma,\text{SM}}$ and c_V . The blue, pink and beige colors show the 1-sigma allowed regions due to gluon fusion $h \rightarrow \gamma\gamma$, $h \rightarrow ZZ^* \rightarrow 4l$ and VBF $h \rightarrow \gamma\gamma$ respectively. The green region is the one favored at 90% CL. In Fig 2a we allow only the Higgs couplings to gluons and photons to change while keeping the other couplings at the SM values. In the remaining plots of Fig 2 we keep $\delta c_\gamma/\delta c_g = 2/9$ fixed, while varying the other couplings. That ratio is conserved when top partners with the same charge and color as the top are introduced.

In the next three sections, we study various models that allow for an improvement in the fine-tuning of the Higgs mass. Our goal is to keep the discussion quite general, and we therefore consider simplified models that capture different paradigms showing up in many models that solve the fine-tuning problem. Each of the models is then mapped on to the effective theory, Eq. (2.1), and the constraints derived above are used to place bounds on the specific scenarios.

4 Models with Scalar Top Partners

4.1 One Scalar

We start our exploration with the simple case of a single scalar top partner. Consider a scalar \tilde{t} with electric charge $2/3$ and transforming in the fundamental representation under the $SU(3)$ color. At the renormalizable level, the top sector mass and interaction terms can

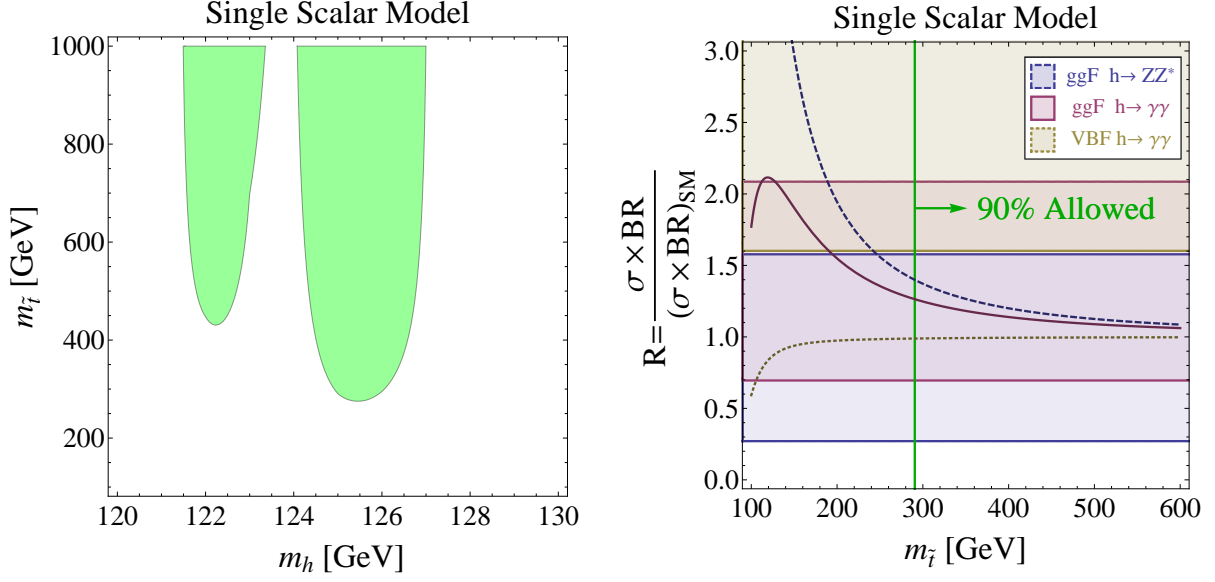


Figure 3: **Left:** Favored region, 90% CL, in the $m_{\tilde{t}} - m_h$ plane, derived from the combination of the three search channels, for the one-scalar model described in Sec. 4.1. **Right:** Constraints for $m_h = 125$ GeV. The three bands show the 1σ allowed regions from Higgs produced via gluon fusion decaying to two photons (ggF $h \rightarrow \gamma\gamma$, pink), Higgs produced via gluon fusion decaying through two Z-bosons (ggF $h \rightarrow ZZ^*$, blue), and Higgs produced via vector boson fusion decaying to two photons (VBF $h \rightarrow \gamma\gamma$, beige). The three curves show the theoretical predictions as a function of $m_{\tilde{t}}$: ggF $h \rightarrow \gamma\gamma$ (solid-pink), ggF $h \rightarrow ZZ$ (dashed-blue), and VBF $h \rightarrow \gamma\gamma$ (dotted-beige). The region to the right of the green line at $m_{\tilde{t}} = 300$ GeV shows the 90% CL experimental (combined) bound.

be parametrized as

$$\mathcal{L}_{stop} = -(yHQ t^c + \text{h.c.}) - |\tilde{t}|^2 (M^2 + \lambda|H|^2). \quad (4.1)$$

Here $Q = (t, b)$ is the 3rd generation quark doublet, t^c is the $SU(2)_W$ singlet top and H is the Higgs doublet. In the unitary gauge $H = (0, (v + h)/\sqrt{2})$ and $|H| = (v + h)/\sqrt{2}$, where $v = 246$ GeV and h is the canonically normalized Higgs boson field. It follows that $m_{\tilde{t}}^2 = M^2 + \lambda v^2/2$. The quadratic divergent top contribution to the Higgs mass is canceled by the scalar partner when the coupling $g_{\tilde{t}}$ is related to the top Yukawa coupling by

$$\lambda = 2y^2. \quad (4.2)$$

For $m_{\tilde{t}} \gg m_h/2$, using Eqs. (2.7),(2.8) one finds the scalar partner contribution to the effective dimension 5 operator,

$$\frac{c_g}{c_{g,\text{SM}}} = \frac{c_\gamma}{c_{\gamma,\text{SM}}} \simeq 1 + \lambda \frac{v^2}{8m_{\tilde{t}}^2} = 1 + \frac{m_t^2}{2m_{\tilde{t}}^2}, \quad c_V = c_b = 1. \quad (4.3)$$

The last equality holds when Eq. (4.2) is satisfied. Thus, if the scalar top partner is solely responsible for the cancellation of the top quadratic divergence, then the gluon fusion rate is always *enhanced*, while the diphoton rate is slightly suppressed for realistic $m_{\tilde{t}}$ (due to interference with the negative W loop contribution). This is unlike the MSSM where both enhancement and suppression of the gluon fusion can be realized within the realistic parameter space (see below).

In Fig. 3 we show the 90% CL allowed region for $m_{\tilde{t}}$ as a function of the Higgs mass (left), along with the 1σ bounds for $m_h = 125$ GeV (right). We see that model independently, a single scalar top partner lighter than 300 GeV is excluded, if indeed the ATLAS and CMS signals correspond to a 125 GeV Higgs boson, as hinted by the data. As can further be seen on the left of Fig. 3, if the Higgs mass is lighter than 122 GeV or heavier than 127 GeV, a heavy stop is excluded as it enhances the gluon-fusion cross-section which is disfavored by the data (see Fig. 1). Similarly, a heavy stop is disfavored at 90% CL for a 124 GeV Higgs boson, due to the VBF measurement by CMS.

4.2 Two Scalars (MSSM)

Consider the system of 2 scalar top partners \tilde{t}, \tilde{t}^c , one for the left-handed top and one for the right-handed top, with the mass terms of the form

$$-\mathcal{L}_{\text{stop}} = |\tilde{t}|^2 (\tilde{m}^2 + y^2 |H|^2) + |\tilde{t}^c|^2 (\tilde{m}_c^2 + y^2 |H|^2) + y |H| X_t (\tilde{t} \tilde{t}^c + \text{h.c.}), \quad (4.4)$$

where y is the top Yukawa coupling, as in Eq. (4.1). This is equivalent to the stop sector of the MSSM in the decoupling limit ($M_A \gg M_Z$) and neglecting the (sub-leading) D-terms contribution to the stop masses. Here the contributions of both scalars sum to cancel the quadratic divergence from the top quark. The left-handed and right-handed stops mix in the presence of X_t , which in the MSSM is given by $X_t = |A_t - \mu \cot \beta|$. See e.g [16].

Denoting the two mass eigenvalues by $m_{\tilde{t}_i}$, and the left-right mixing angle by θ_t , one has

$$m_t X_t = \frac{1}{2} (m_{\tilde{t}_2}^2 - m_{\tilde{t}_1}^2) \sin 2\theta_t \quad (4.5)$$

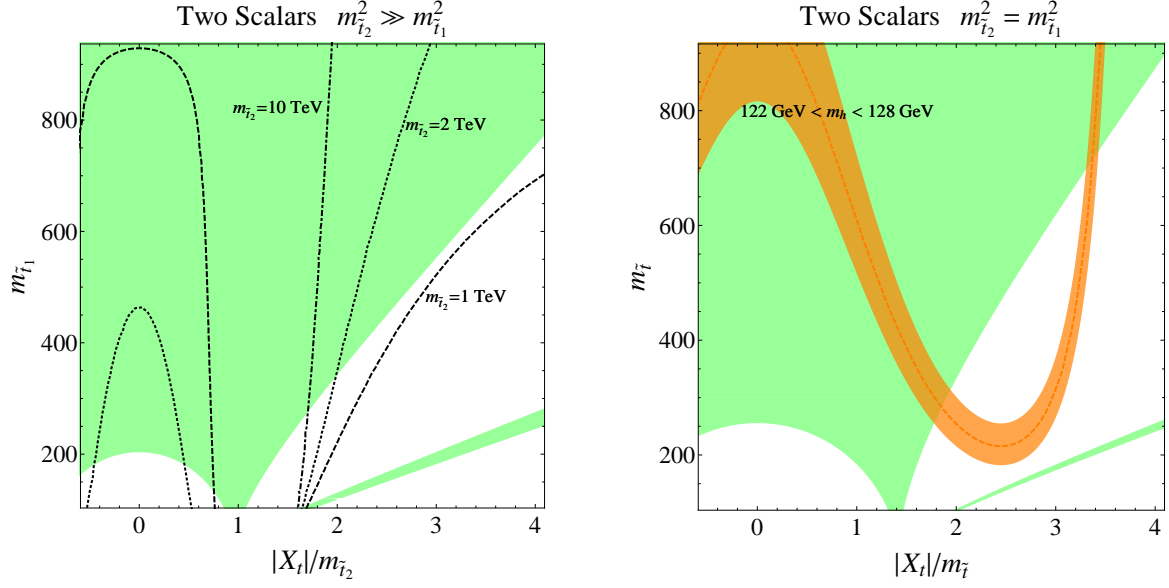


Figure 4: **Left:** The favored region at 90% CL for $m_h = 125$ GeV, derived from the combination of the three search channels, in the two scalar model with $m_{t_2} \gg m_{t_1}$. Also shown are contours of constant $m_h = 125$ GeV assuming the 1-loop MSSM relation between Higgs and stop masses, for $m_{t_2} = 1, 2$, and 10 TeV. **Right:** Same for $m_{t_2} = m_{t_1}$. Also shown is a band corresponding to $122 \text{ GeV} < m_h < 128 \text{ GeV}$ assuming the 1-loop MSSM relation between Higgs and stop masses. Additional, model-dependent, bounds on stops from direct searches are not shown.

where, by convention, $m_{t_1} \leq m_{t_2}$. For $m_{t_i} \gg m_h/2$, integrating out the stops shifts the effective dimension-5 operators as

$$\frac{c_g}{c_{g,\text{SM}}} = \frac{c_\gamma}{c_{\gamma,\text{SM}}} = 1 + \frac{1}{4} \left(\frac{m_t^2}{m_{t_1}^2} + \frac{m_t^2}{m_{t_2}^2} - \frac{m_t^2 X_t^2}{m_{t_1}^2 m_{t_2}^2} \right) \quad (4.6)$$

For zero mixing, the stops always interfere constructively with the top contribution (destructively with the W -contribution to \hat{c}_γ), but once X_t becomes comparable to stop masses an enhancement of c_g becomes possible. A significant shift of the gluon fusion and diphoton widths is possible if at least one of the stop mass eigenvalues is close to the top mass, or if the mixing is very large.

In Fig. 4 we illustrate the impact of the LHC Higgs data on the parameter space of the 2-scalar-partner model. The left plot shows the allowed region in the $m_{t_1}^2 - X_t^2/m_{t_2}^2$ plane, assuming that $m_{t_2}^2$ is large enough so that the heavier stop eigenstate does not contribute to

the effective operators (that is, dropping the second term in the bracket in Eq. (4.6)). For no mixing, $X_t^2/m_{\tilde{t}_2}^2 = 0$, the lower bound on the lightest stop is ~ 210 GeV. This bound is weaker than the one in the single partner model because the coupling of each stop is a factor of 2 smaller. On the right plot we consider the case of degenerate stops. Here, for no mixing, we get the same bound on the stop mass as in the single partner model.

In both scenarios, for just right amount of mixing, that is $X_t/m_{\tilde{t}_2} \simeq 1$ for $m_{\tilde{t}_2}^2 \gg m_{\tilde{t}_1}^2$ and $|X_t|/m_{\tilde{t}_2} \simeq \sqrt{2}$ for $m_{\tilde{t}_2}^2 = m_{\tilde{t}_1}^2$, the scalar partners contribution to c_g and c_γ can vanish, even for very light stops. This may be relevant for models that require a light stop, such as electroweak baryogenesis [17]. For illustration, on the left plot of Fig. 4 we show contours of constant $m_h = 125$ GeV, for $m_{\tilde{t}_2} = 1, 2$, and 10 TeV, while on the right plot we show the region where $123 \text{ GeV} < m_h < 128 \text{ GeV}$. As a final remark, we comment that additional bounds on stops exist from direct searches. These bounds are however model dependent, in particular strongly depending on the stop decay branching fractions, and therefore we do not display them.

5 Models with a Fermionic Top Partner

We move to the case of one fermionic top partner. Consider the SM model extended by a vector-like quark pair (T, T^c) in the $\mathbf{1}_{2/3}$ representation under $SU(2)_W \times U(1)_Y$. Fermionic partners cannot cancel the top quadratic divergence if the effective Lagrangian describing their interactions with the Higgs is renormalizable. Therefore in this case we need to consider a more general effective Lagrangian for the top sector that includes non-renormalizable interactions,

$$-\mathcal{L}_{top} = y_1(|H|^2)HQt^c + y_2(|H|^2)HQT^c + M_1(|H|^2)Tt^c + M_2(|H|^2)TT^c + \text{h.c.} \quad (5.1)$$

We allow the vacuum expectation value of the Higgs doublet, \hat{v} , to be different from the electroweak scale $v = 246$ GeV, which may happen if the Higgs effective interactions with W/Z bosons are also non-renormalizable and corresponds to $c_V \neq 1$ (this is in fact the case in Little Higgs and composite Higgs models). We assume that all mass and Yukawa couplings are functions of $|H|^2$ and can be expanded in powers of $|H|^2/M^2$ where M is the mass scale

of the heavy top quark. Up to order $|H|^2/M^2$ they can be parametrized as

$$y_1(|H|^2) = y_1 \left(1 - d_1 \frac{|H|^2}{M^2} \right) + \mathcal{O}\left(\frac{|H|^4}{M^4}\right), \quad (5.2)$$

$$y_2(|H|^2) = y_2 \left(1 - d_2 \frac{|H|^2}{M^2} \right) + \mathcal{O}\left(\frac{|H|^4}{M^4}\right), \quad (5.3)$$

$$M_1(|H|^2) = c_1 M \frac{|H|^2}{M^2} + \mathcal{O}\left(\frac{|H|^4}{M^4}\right), \quad (5.4)$$

$$M_2(|H|^2) = M \left(1 - c_2 \frac{|H|^2}{M^2} \right) + \mathcal{O}\left(\frac{|H|^4}{M^4}\right). \quad (5.5)$$

Above, we used the freedom to rotate t^c and T^c such that M_1 starts at $\mathcal{O}(|H|^2)$. In terms of these parameters $m_{top} \simeq y_1 \hat{v}/\sqrt{2}$ while $m_T \simeq M$. For the cancellation of the quadratic divergences in the Higgs mass term, one straightforwardly finds,

$$c_2 = \frac{y_1^2 + y_2^2}{2}. \quad (5.6)$$

This relation may arise naturally in models where the Higgs is realized as a pseudo-Goldstone boson of a spontaneously broken approximate global symmetry.

Following the discussion above Eq. (2.7) and integrating out the top sector, one finds for the effective Higgs coupling to gluons and photons shifts as

$$\frac{c_g}{c_{g,\text{SM}}} = \frac{c_\gamma}{c_{\gamma,\text{SM}}} \simeq \frac{v}{\hat{v}} \left[1 - \frac{\hat{v}^2}{M^2} \left(d_1 + c_2 + \frac{c_1 y_2}{y_1} \right) \right]. \quad (5.7)$$

We see that several parameters of the effective Lagrangian enter the modification of effective Higgs coupling to gluons and photons. Above, y_1 can be eliminated in favor of the top mass, and c_2 can be eliminated using the condition Eq. (5.6). This still leaves 4 free parameters: d_1 , y_2 , \hat{v}/v and M . Thus, in full generality, we cannot predict the magnitude, or even the sign of the correction to the Higgs rate merely by demanding cancellation of quadratic divergences.⁴ However, concrete realizations of Little Higgs and composite Higgs models often imply additional relations between the effective theory parameters, in which case the set-up becomes more predictive. Below we study several predictive patterns of effective theory parameters that arise in popular Little Higgs and composite Higgs models.

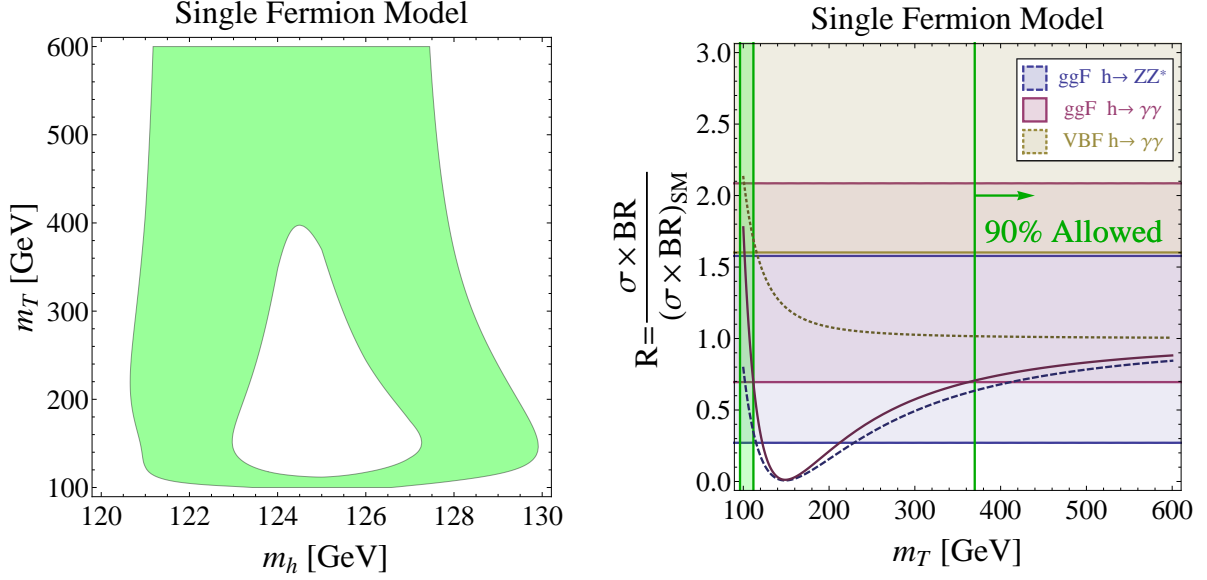


Figure 5: **Left:** Favored region, 90% CL, in the $m_T - m_h$ plane, derived from the combination of the three search channels, for the single-fermion, no-mixing model described in Sec. 5.1. **Right:** Constraints assuming $m_h = 125$ GeV. The three bands show the 1σ allowed regions from Higgs produced via gluon fusion (ggF) decaying to $\gamma\gamma$ (pink), or to $ZZ^* \rightarrow 4l$ (blue), and Higgs produced via vector boson fusion (VBF) decaying to $\gamma\gamma$ (beige). The three curves show the theoretical predictions as a function of m_T ggF $h \rightarrow \gamma\gamma$ (solid-pink), ggF $h \rightarrow ZZ$ (dashed-blue) and VBF $h \rightarrow \gamma\gamma$ (dotted-beige). The region to the right of the green line at $m_T = 350$ GeV shows the 90% CL experimental (combined) allowed region. There is also a small region allowed by the Higgs searches, around $m_T = 100$ GeV, that is highly constrained by other, model-dependent, experimental results not presented here.

5.1 No mixing

First, we will restrict the parameter space by demanding that the SM top does not mix with its partners, $c_1 = y_2 = 0$, and $c_2 = y_1^2/2 \simeq m_t^2/v^2$. This situation occurs in Little Higgs with T-parity [18]. Furthermore, we assume that the Higgs coupling to the SM fields is not modified at $\mathcal{O}(v^3)$, thus $\hat{v} = v$ and $d_1 = 0$. Under these assumptions one finds

$$\frac{c_g}{c_{g,\text{SM}}} = \frac{c_\gamma}{c_{\gamma,\text{SM}}} \simeq 1 - \frac{m_t^2}{m_T^2}, \quad c_V = c_b = 1. \quad (5.8)$$

Hence in this scenario, much as in the case of one scalar partner, the departure of the Higgs rates from the SM can be described by one parameter: the ratio of the top mass to its partner mass. The gluon width, and in consequence the dominant Higgs production mode, is reduced. On the other hand, the Higgs partial width into WW and ZZ are unchanged, while the partial width in the $\gamma\gamma$ channel is significantly changed only when $m_T \sim m_t$. In Fig. 5 we present the constraints on m_T from the LHC Higgs data. In the left plot we show the 90% CL allowed region, in the m_h - m_T plane. The right plot shows the constraints assuming a 125 GeV Higgs. As can be seen, $m_T \lesssim 350$ GeV is disfavored in this case except for a small band around 100 GeV, which in most models would be difficult to reconcile with the constraints from direct searches.

5.2 Universal suppression

Consider now a frequently occurring situation when all the Higgs rates are suppressed by a universal factor depending on the compositeness scale f . To be specific, consider the top sector interacting with a pseudo-Goldstone Higgs as

$$- \mathcal{L}_{top} = yf \sin(|H|/f) tt^c + yf \cos(|H|/f) Tt^c + M' TT^c + \text{h.c.} \quad (5.9)$$

The top partner mass is of order $m_T \simeq \sqrt{y^2 f^2 + M'^2}$. Integrating out the top sector we find,

$$\frac{c_g}{c_{g,\text{SM}}} = \frac{c_\gamma}{c_{\gamma,\text{SM}}} = \cos(\hat{v}/\sqrt{2}f) = \sqrt{1 - \frac{v^2}{2f^2}}. \quad (5.10)$$

⁴In composite Higgs models under certain conditions one can argue that the gluon fusion and diphoton decay rate cannot be enhanced [19].

Thus, the top sector contribution to the Higgs dimension-5 interactions is reduced by a factor that is independent of the details of the top sector, such as the masses and the coupling of the top eigenstates. The interaction terms in Eq. (5.9) arise e.g. in the Simplest Little Higgs model with an $[SU(3)/SU(2)]^2$ coset structure [20] when taking the limit $f_2 \gg f_1$. In that case one also finds $c_V = c_b = \sqrt{1 - \frac{v^2}{2f^2}}$. Therefore, in the Simplest Little Higgs model, the rates in all Higgs channels are universally suppressed by a factor depending only on the compositeness scale: $\sigma/\sigma_{SM} = 1 - v^2/2f^2$. The same holds for the $SO(5)/SO(4)$ minimal composite Higgs with fermions embedded in the spinorial representation of $SO(5)$ [21]. Note that the independence of the Higgs widths of the fine details of the top sector persists in numerous Little Higgs and composite Higgs models [22], although it may not hold in more complicated models where the top couples to more than one composite operator [23].

Repeating the analysis done in previous sections, in Fig. 6 we present the constraints on $\xi \equiv v^2/f^2$ from the current LHC Higgs measurements. We find that, assuming a 125 GeV Higgs boson, $\xi > 0.5$ is excluded at the 90% CL. Note that as discussed above, all relative rates have similar dependence on ξ and are therefore on drawn on top of one another.

5.3 Non-universal suppression

Another phenomenologically distinct example with one top partner arises within the Twin Higgs scenario [24], where the global symmetry giving rise to a pseudo-Goldstone Higgs arises accidentally as a consequence of a discrete symmetry. In particular, in the left-right symmetric Twin Higgs model [25] the top sector interactions with the Higgs take the form

$$-\mathcal{L}_{top} = y \sin(|H|/f) t T^c + y \cos(|H|/f) T t^c + M_2 T T_c. \quad (5.11)$$

Using the same methods as before one finds,

$$c_V = c_b = \sqrt{1 - \frac{v^2}{2f^2}}, \quad \frac{c_g}{c_{g,SM}} = \frac{c_\gamma}{c_{\gamma,SM}} = \frac{1 - \frac{v^2}{f^2}}{\sqrt{1 - \frac{v^2}{2f^2}}}. \quad (5.12)$$

In this example, the Higgs partial width into gluons is modified by a different factor than that into W and Z bosons. The constraints on the non-universal suppression models are presented in Fig. 7.

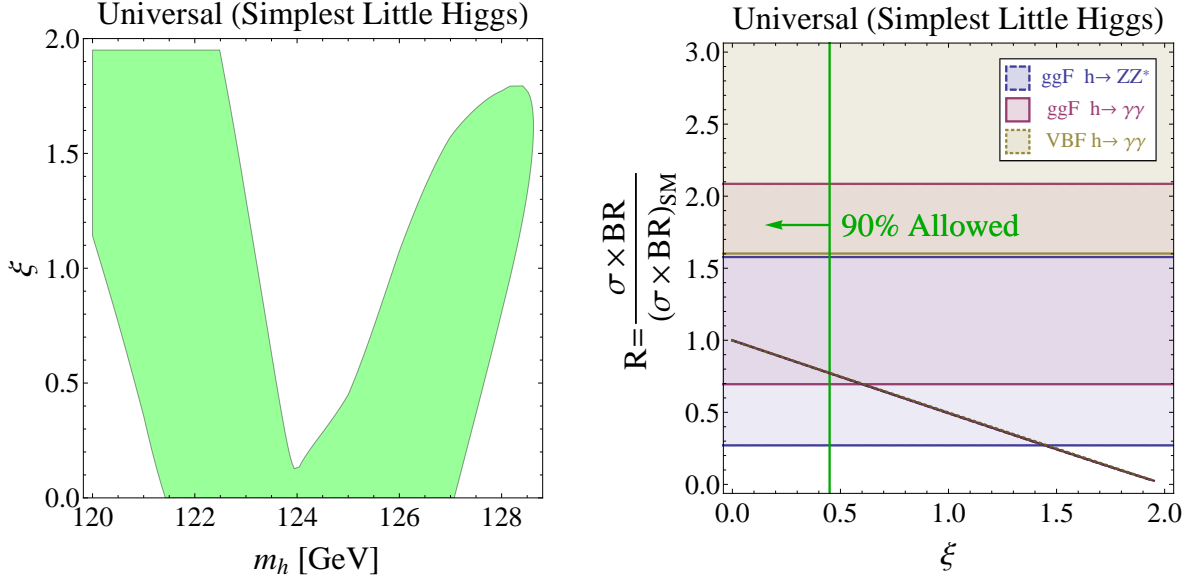


Figure 6: **Left:** Favored region, 90% CL, in the $\xi - m_h$ plane where $\xi \equiv \frac{v^2}{f^2}$, derived from the combination of the three search channels, for models with universal suppression such as the Simplest Little Higgs model described in Sec. 5.2. **Right:** Constraints for $m_h = 125$ GeV. The three bands show the 1σ allowed regions from Higgs produced via gluon fusion (ggF) decaying to $\gamma\gamma$ (pink), or to $ZZ^* \rightarrow 4l$ (blue), and Higgs produced via vector boson fusion (VBF) decaying to $\gamma\gamma$ (beige). The three curves show the theoretical predictions as a function of m_T : ggF $h \rightarrow \gamma\gamma$ (solid-pink), ggF $h \rightarrow ZZ^* \rightarrow 4l$ (dashed-blue) and VBF $h \rightarrow \gamma\gamma$ (dotted-beige). Due to the universal suppression all three curves share the same dependence on ξ and are therefore on top of one another. The region to the left of the green line at $\xi \simeq 0.45$ shows the 90% CL experimental (combined) allowed region.

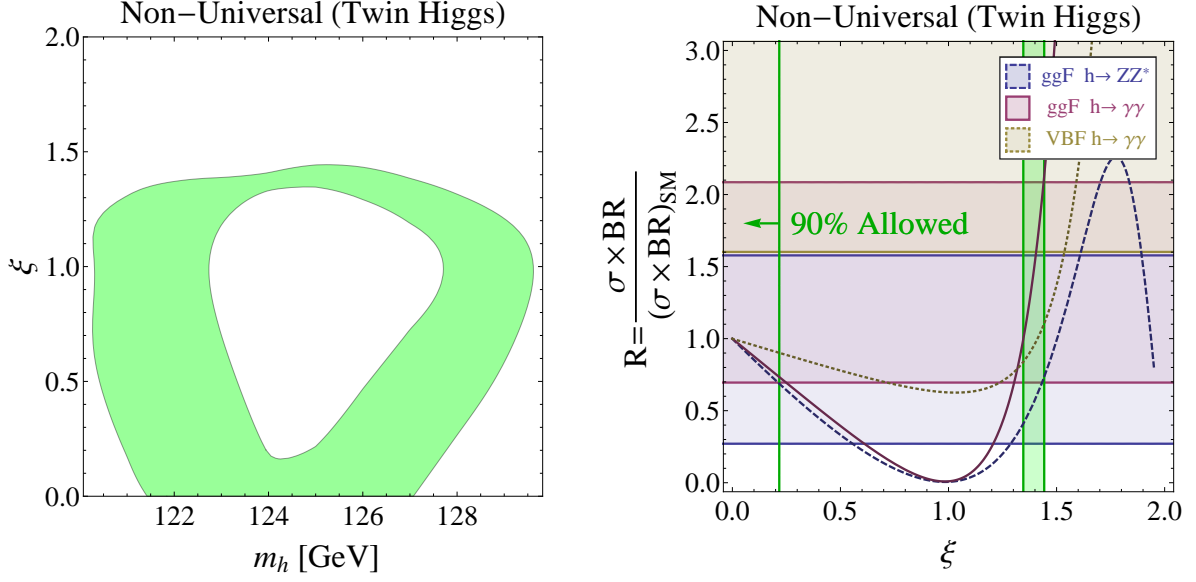


Figure 7: **Left:** Favored region, 90% CL, in the $\xi \equiv \frac{v^2}{f^2} - m_h$ plane, derived from the combination of the three search channels, for the Twin Higgs model described in Sec. 5.3. **Right:** Constraints for $m_h = 125$ GeV. The three bands show the 1σ allowed regions from Higgs produced via gluon fusion (ggF) decaying to $\gamma\gamma$ (pink), or to $ZZ^* \rightarrow 4l$ (blue), and Higgs produced via vector boson fusion (VBF) decaying to $\gamma\gamma$ (beige). The three curves show the theoretical predictions as a function of m_T : ggF $h \rightarrow \gamma\gamma$ (solid-pink), ggF $h \rightarrow ZZ$ (dashed-blue) and VBF $h \rightarrow \gamma\gamma$ (dotted-beige). The region to the left of the green line at $\xi \simeq 0.23$ shows the 90% CL experimental (combined) allowed region.

6 Multi-Higgs models

6.1 Doublet + Singlet

The simplest set-up with multiple Higgs bosons is the one with an electroweak-singlet scalar field mixing with the Higgs. As a result, the mass eigenstates are linear combinations of the Higgs scalar originating from the doublet (which couples to the SM matter) and singlet (which does not couple to matter). Denoting the mixing angle as α , all the couplings of the Higgs boson are suppressed by $\cos \alpha$,

$$c_V = c_b = \frac{c_g}{c_{g,\text{SM}}} = \frac{c_\gamma}{c_{\gamma,\text{SM}}} = \cos \alpha. \quad (6.1)$$

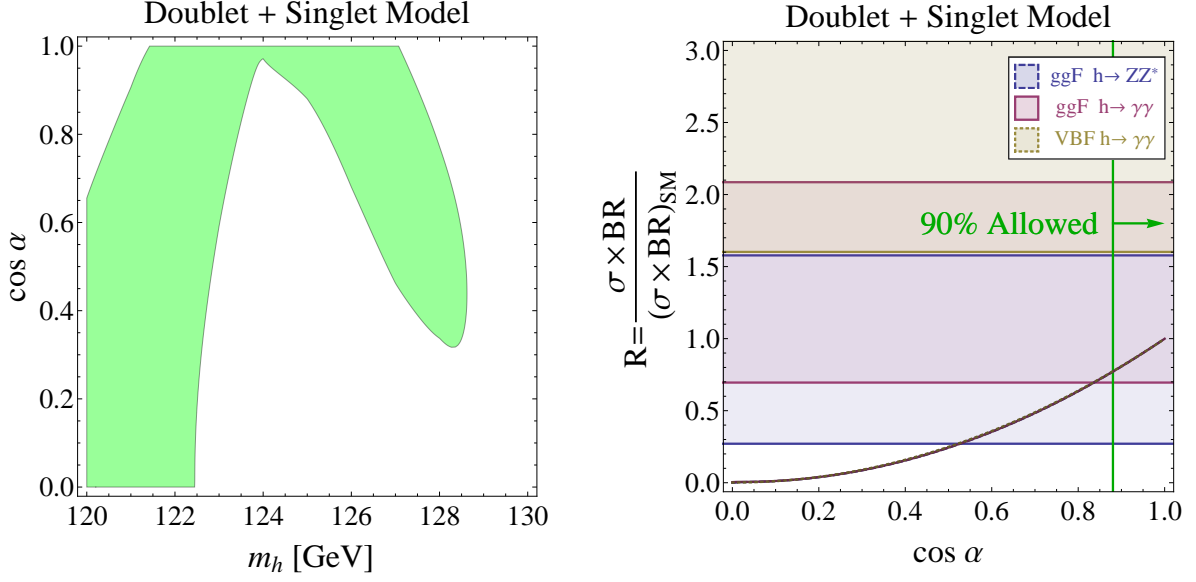


Figure 8: **Left:** Favored region, 90% CL, in the $\cos \alpha - m_h$ plane, derived from the combination of the three search channels, for the doublet-singlet model described in Sec. 6.1. **Right:** Constraints for $m_h = 125$ GeV. The three bands show the 1σ allowed regions from Higgs produced via gluon fusion (ggF) decaying to $\gamma\gamma$ (pink), or to $ZZ^* \rightarrow 4l$ (blue), and Higgs produced via vector boson fusion (VBF) decaying to $\gamma\gamma$ (beige). The three curves show the theoretical predictions as a function of $\cos \alpha$: ggF $h \rightarrow \gamma\gamma$ (solid-pink), ggF $h \rightarrow ZZ$ (dashed-blue) and VBF $h \rightarrow \gamma\gamma$ (dotted-beige). The region to the right of the green line at $\xi \simeq 0.86$ shows the 90% CL experimental (combined) allowed region.

As a consequence, the Higgs production and decay rates in all the channels are universally suppressed by $\cos^2 \alpha$. This is analogous to what happens in a fermionic model in Section 5.2. The new element is the appearance of the second Higgs eigenstate, denoted by H^0 , whose couplings are suppressed by $\sin \alpha$ compared to those of the SM Higgs boson, and whose mass is in general a free parameter. In Fig. 8 we present the LHC Higgs constraints on this model. We find rather strong constraints on the mixing of the doublet with the singlet, $\cos \alpha \gtrsim 0.88$. In deriving these constraints we assumed that $m_{H^0} > m_h/2$.

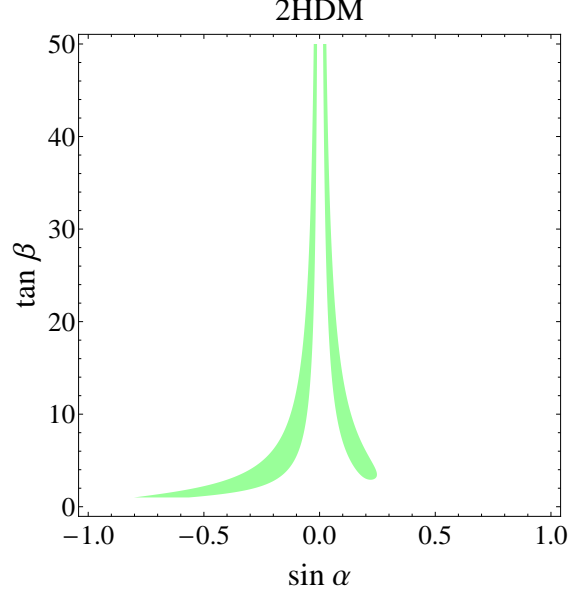


Figure 9: Favored region, 90% CL, of the 2HDM in the $\tan \beta - \sin \alpha$ plane, derived from the combination of the three search channels. We take $m_{H^\pm} = 200$ GeV, but a lighter charged Higgs would only slightly change the favored region. The favored region for $\sin \alpha < 0$ concentrates around the decoupling limit, $\alpha = \beta - \pi/2$, where all couplings are SM-like, whereas the region for $\sin \alpha > 0$ lies around the region $\alpha = -\beta + \pi/2$ where the top Yukawa coupling is SM-like.

6.2 Two Higgs Doublets

We end with the study of 2 Higgs doublets H_u , H_d , the former coupling to up-type quarks, and the latter to down-type quarks and leptons. The physical fields are embedded into the doublets as,

$$H_u = \begin{pmatrix} \cos \beta H^+ \\ \frac{1}{\sqrt{2}}(v \sin \beta + h \cos \alpha + H^0 \sin \alpha + i A^0 \cos \beta) \end{pmatrix}, \quad (6.2)$$

$$H_d = \begin{pmatrix} \frac{1}{\sqrt{2}}(v \cos \beta - h \sin \alpha + H^0 \cos \alpha + i A^0 \sin \beta) \\ \sin \beta H^- \end{pmatrix}. \quad (6.3)$$

The couplings of the lightest Higgs boson h are described by two angle α, β who are in general free parameters⁵. We find,

$$c_V = \sin(\beta - \alpha), \quad c_b = -\frac{\sin \alpha}{\cos \beta}, \quad \frac{c_g}{c_{g,\text{SM}}} = \frac{c_\gamma}{c_{\gamma,\text{SM}}} = \frac{\cos \alpha}{\sin \beta}. \quad (6.4)$$

By convention $0 < \beta < \pi/2$. In general, there is an additional contribution to c_γ from the charged Higgs, but it is always small compared to the contribution from the W-boson.

The 2 Higgs Doublet Model (2HDM) can change all couplings to the Higgs and thus is highly constrained by the LHC Higgs searches [9, 26]. In Fig. 9 we show the constraints in the $\tan \beta - \sin \alpha$ plane for $m_{H^\pm} = 200$ GeV. Lighter masses would only slightly change the favored region. The favored region for $\sin \alpha < 0$ concentrates around the decoupling limit $\alpha = \beta - \pi/2$, where all couplings are SM-like. The region for $\sin \alpha > 0$ lies around the region $\alpha = -\beta + \pi/2$ where the top Yukawa coupling is SM-like.

7 Conclusions

The indications for the existence of a Higgs boson provided recently by ATLAS and CMS are preliminary and may go away with more data. With this caveat in mind, it is interesting to ask whether the available experimental information is compatible with the SM Higgs boson, and whether it favors or disfavors any particular constructions beyond the SM. In this paper we analyzed recent LHC searches sensitive to a light (115-130 GeV) Higgs boson, combining results in the $h \rightarrow \gamma\gamma$ channel (both gluon fusion and vector-boson fusion) and $h \rightarrow ZZ^* \rightarrow 4l$ channel, as well as combining the ATLAS and CMS data. We presented interpretations of that combination in the context of several effective models, with the special emphasis on models addressing the naturalness problem of electroweak symmetry breaking.

We have argued that, unsurprisingly, combination of the ATLAS and CMS data favors the Higgs boson in the mass range 124 – 126 GeV, with the best fit cross section close to the one predicted by the SM. Less trivially, we recast the LHC Higgs results as constraints on the parameters of the effective lagrangian at the scale $\sim m_h$ describing the leading interactions of the Higgs boson with the SM fields. Furthermore, we found that the LHC Higgs data

⁵If the Higgs potential is that of the MSSM, the angle α is not independent of m_{A^0} and m_{H^\pm} . Furthermore, in that case $-\pi/2 < \alpha < 0$ for $m_{A^0} > m_Z$.

already put interesting constraints on simple natural new physics models, especially on those predicting suppression of $\sigma(pp \rightarrow h)\text{Br}(h \rightarrow \gamma\gamma)$ and $\sigma(pp \rightarrow h jj)\text{Br}(h \rightarrow \gamma\gamma)$. For example, in a model with one fermionic top partner stabilizing the Higgs potential, the top partner masses below ~ 350 GeV are disfavored at 90% CL. For one scalar partner the corresponding bound is weaker, ~ 300 GeV, due to the fact that a single scalar stabilizing the Higgs potential always provides a positive contribution to $\Gamma(h \rightarrow \gamma\gamma)$. These bounds can be further relaxed for more complicated models. In particular in a model with 2 scalar partners the total contribution to $\Gamma(h \rightarrow \gamma\gamma)$ can be negligible even for very light scalars, at the expense of fine tuning.

We anticipate these bounds to significantly improve with additional data to be collected in 2012. Alternatively, studying the effective theory of the Higgs bosons may prove to be the shortest way to a discovery of new physics beyond the SM.

Note added: Right after our paper appeared, Refs. [27] and [28] also appeared. The references also interpret the LHC Higgs results as constraints on the effective theory of Higgs interactions and overlap in part with our work. In order to assess compatibility with our results, in v2 we added the top right plot of Fig. 2, which can be directly compared to the contours in the $a-c$ plane presented in [27, 28]. In spite of using different statistical methods, we find very similar preferred regions in the $a-c$ plane. Nevertheless, our constraints on $\xi = v^2/f^2$ in Section 5.2 are somewhat stronger than in [27]. We further note that our definition of ξ differs by a factor of 2 compared to the definition in [27, 28].

Acknowledgements

We especially thank Patrick Meade for collaboration in the early stages of this project and for many useful discussions. We also thank David Curtin, Aielet Efrati, Yonit Hochberg, Yossi Nir and Gilad Perez for useful discussions. The work of DC, EK and TV is supported in part by a grant from the Israel Science Foundation. The work of TV is further supported in part by the US-Israel Binational Science Foundation and the EU-FP7 Marie Curie, CIG fellowship.

References

- [1] ATLAS Collaboration, arXiv:1202.1408 [hep-ex]. S. Chatrchyan *et al.* [CMS Collaboration], arXiv:1202.1488 [hep-ex].
- [2] ATLAS Collaboration, arXiv:1202.1414 [hep-ex].
- [3] ATLAS Collaboration, arXiv:1202.1415 [hep-ex].
- [4] S. Chatrchyan *et al.* [CMS Collaboration], arXiv:1202.1487 [hep-ex].
- [5] S. Chatrchyan *et al.* [CMS Collaboration], arXiv:1202.1997 [hep-ex].
- [6] S. Chatrchyan *et al.* [CMS Collaboration], arXiv:1202.1489 [hep-ex]. S. Chatrchyan *et al.* [CMS Collaboration], arXiv:1202.1416 [hep-ex].
- [7] J. R. Espinosa, C. Grojean and M. Muehlleitner, arXiv:1202.1286 [hep-ph].
- [8] L. J. Hall, D. Pinner and J. T. Ruderman, arXiv:1112.2703 [hep-ph]. A. Arbey, M. Battaglia, A. Djouadi, F. Mahmoudi and J. Quevillon, Phys. Lett. B **708**, 162 (2012) [arXiv:1112.3028 [hep-ph]]. S. Heinemeyer, O. Stal and G. Weiglein, arXiv:1112.3026 [hep-ph]. P. Draper, P. Meade, M. Reece and D. Shih, arXiv:1112.3068 [hep-ph]. M. Carena, S. Gori, N. R. Shah and C. E. M. Wagner, arXiv:1112.3336 [hep-ph]. U. Ellwanger, arXiv:1112.3548 [hep-ph]. M. Kadastik, K. Kannike, A. Racioppi and M. Raidal, arXiv:1112.3647 [hep-ph]. J. Cao, Z. Heng, D. Li and J. M. Yang, arXiv:1112.4391 [hep-ph]. A. Arvanitaki and G. Villadoro, arXiv:1112.4835 [hep-ph]. J. F. Gunion, Y. Jiang and S. Kraml, arXiv:1201.0982 [hep-ph]. S. F. King, M. Muehlleitner and R. Nevzorov, arXiv:1201.2671 [hep-ph]. Z. Kang, J. Li and T. Li, arXiv:1201.5305 [hep-ph].
- [9] P. M. Ferreira, R. Santos, M. Sher and J. P. Silva, arXiv:1112.3277 [hep-ph]. P. M. Ferreira, R. Santos, M. Sher and J. P. Silva, arXiv:1201.0019 [hep-ph]. E. Cervero and J. M. Gerard, arXiv:1202.1973 [hep-ph]. K. Blum and R. T. D’Agnolo, arXiv:1202.2364 [hep-ph].
- [10] C. Englert, T. Plehn, M. Rauch, D. Zerwas and P. M. Zerwas, Phys. Lett. B **707** (2012) 512 [arXiv:1112.3007 [hep-ph]]. C. Cheung and Y. Nomura, arXiv:1112.3043 [hep-ph].

- G. Guo, B. Ren and X. -G. He, arXiv:1112.3188 [hep-ph]. A. Djouadi, O. Lebedev, Y. Mambrini and J. Quevillon, arXiv:1112.3299 [hep-ph]. K. Cheung and T. -C. Yuan, arXiv:1112.4146 [hep-ph]. B. Batell, S. Gori and L. -T. Wang, arXiv:1112.5180 [hep-ph]. A. Falkowski, S. Rychkov and A. Urbano, arXiv:1202.1532 [hep-ph]. E. Gabrielli, B. Mele and M. Raidal, arXiv:1202.1796 [hep-ph].
- [11] F. Bonnet, M. B. Gavela, T. Ota and W. Winter, arXiv:1105.5140 [hep-ph]. C. Englert, T. Plehn, D. Zerwas and P. M. Zerwas, “Exploring the Higgs Portal,” Phys. Lett. B **703** (2011) 298 [arXiv:1106.3097 [hep-ph]]. C. Englert, J. Jaeckel, E. Re and M. Spannowsky, arXiv:1111.1719 [hep-ph]. B. A. Dobrescu, G. D. Kribs and A. Martin, arXiv:1112.2208 [hep-ph]. A. Drozd, B. Grzadkowski and J. Wudka, arXiv:1112.2582 [hep-ph].
- [12] A. Djouadi, Phys. Rept. **457**, 1 (2008) [hep-ph/0503172]. A. Djouadi, Phys. Rept. **459** (2008) 1 [arXiv:hep-ph/0503173].
- [13] J. R. Ellis, M. K. Gaillard and D. V. Nanopoulos, Nucl. Phys. B **106**, 292 (1976). M. A. Shifman, A. I. Vainshtein, M. B. Voloshin and V. I. Zakharov, Sov. J. Nucl. Phys. **30**, 711 (1979) [Yad. Fiz. **30**, 1368 (1979)].
- [14] J. Alwall, M. Herquet, F. Maltoni, O. Mattelaer and T. Stelzer, JHEP **1106**, 128 (2011) [arXiv:1106.0522 [hep-ph]].
- [15] S. Ovnyn, X. Roubly and V. Lemaitre, arXiv:0903.2225 [hep-ph].
- [16] R. Dermisek and I. Low, Phys. Rev. D **77**, 035012 (2008) [hep-ph/0701235 [HEP-PH]].
- [17] M. Carena, G. Nardini, M. Quiros and C. E. M. Wagner, Nucl. Phys. B **812**, 243 (2009) [arXiv:0809.3760 [hep-ph]]. T. Cohen and A. Pierce, arXiv:1110.0482 [hep-ph].
- [18] H. C. Cheng and I. Low, JHEP **0309** (2003) 051 [arXiv:hep-ph/0308199]. H. C. Cheng, I. Low and L. T. Wang, Phys. Rev. D **74** (2006) 055001 [arXiv:hep-ph/0510225].
- [19] I. Low, R. Rattazzi and A. Vichi, JHEP **1004** (2010) 126 [arXiv:0907.5413 [hep-ph]].
- [20] M. Schmaltz, JHEP **0408**, 056 (2004) [arXiv:hep-ph/0407143]. D. E. Kaplan and M. Schmaltz, JHEP **0310**, 039 (2003) [hep-ph/0302049]. M. Schmaltz and D. Tucker-Smith, Ann. Rev. Nucl. Part. Sci. **55**, 229 (2005) [hep-ph/0502182]. M. Perelstein, Prog.

- Part. Nucl. Phys. **58**, 247 (2007) [hep-ph/0512128]. T. Han, H. E. Logan, B. McElrath and L. -T. Wang, Phys. Rev. D **67**, 095004 (2003) [hep-ph/0301040]. T. Han, H. E. Logan, B. McElrath and L. -T. Wang, Phys. Lett. B **563**, 191 (2003) [Erratum-ibid. B **603**, 257 (2004)] [hep-ph/0302188].
- [21] K. Agashe, R. Contino and A. Pomarol, Nucl. Phys. B **719**, 165 (2005) [hep-ph/0412089]. J. R. Espinosa, C. Grojean and M. Muhlleitner, JHEP **1005** (2010) 065 [arXiv:1003.3251 [hep-ph]].
- [22] A. Falkowski, Phys. Rev. D **77** (2008) 055018 [arXiv:0711.0828 [hep-ph]]. G. Cacciapaglia, A. Deandrea and J. Llodra-Perez, JHEP **0906**, 054 (2009) [arXiv:0901.0927 [hep-ph]]. I. Low and A. Vichi, Phys. Rev. D **84**, 045019 (2011) [arXiv:1010.2753 [hep-ph]].
- [23] A. Azatov and J. Galloway, arXiv:1110.5646 [hep-ph].
- [24] Z. Chacko, H. S. Goh and R. Harnik, Phys. Rev. Lett. **96** (2006) 231802 [arXiv:hep-ph/0506256].
- [25] Z. Chacko, H. S. Goh and R. Harnik, JHEP **0601** (2006) 108 [arXiv:hep-ph/0512088].
- [26] For some earlier work see e.g. A. G. Akeroyd, J. Phys. G **24** (1998) 1983 [arXiv:hep-ph/9803324]; B. Grzadkowski and P. Osland, Phys. Rev. D **82** (2010) 125026 [arXiv:0910.4068 [hep-ph]].
- [27] A. Azatov, R. Contino and J. Galloway, arXiv:1202.3415 [hep-ph].
- [28] J. R. Espinosa, C. Grojean, M. Muhlleitner and M. Trott, arXiv:1202.3697 [hep-ph].